

A weighted first-order formulation for solving anisotropic diffusion equations with deep neural networks

Hui Xie*, Chuanlei Zhai†, Li Liu‡, Heng Yong§

Abstract

In this paper, a new weighted first-order formulation is proposed for solving the anisotropic diffusion equations with deep neural networks. For many numerical schemes, the accurate approximation of anisotropic heat flux is crucial for the overall accuracy. In this work, the heat flux is firstly decomposed into two components along the two eigenvectors of the diffusion tensor, thus the anisotropic heat flux approximation is converted into the approximation of two isotropic components. Moreover, to handle the possible jump of the diffusion tensor across the interface, the weighted first-order formulation is obtained by multiplying this first-order formulation by a weighted function. By the decaying property of the weighted function, the weighted first-order formulation is always well-defined in the pointwise way. Finally, the weighted first-order formulation is solved with deep neural network approximation. Compared to the neural network approximation with the original second-order elliptic formulation, the proposed method can significantly improve the accuracy, especially for the discontinuous anisotropic diffusion problems.

Keywords. anisotropic diffusion, discontinuous interface, weighted first-order system, deep neural network.

AMS subject classifications. 65N35, 41A46, 35J25.

*Institute of Applied Physics and Computational Mathematics, Beijing, 100094, China(xiehui@lsec.cc.ac.cn)

†Institute of Applied Physics and Computational Mathematics, Beijing, 100094, China(zhai_chuanlei@iapcm.ac.cn)

‡Institute of Applied Physics and Computational Mathematics, Beijing, 100094, China(liu_li@iapcm.ac.cn)

§Institute of Applied Physics and Computational Mathematics, Beijing, 100094, China(yong_heng@iapcm.ac.cn)

1 Introduction

Anisotropic diffusion equations arise from numerical simulations of many important and practical applications such as inertial confinement fusion (ICF) [18, 22], reservoir simulation [30], astrophysical fluid dynamics [26]. Generally, the modelling of the anisotropic diffusion equation is coupled with the fluid dynamics. Particularly, in the Lagrangian reference frame, the computational mesh is moved with the fluid motions. For the traditional discrete schemes, the accuracy is degenerated due to the the distorted meshes and the anisotropic diffusion tensors. In addition, the different materials or local physical field (e.g., magnetic field) in the problems will result in the high discontinuous diffusion tensor across the interface. Even with the Eulerian reference frame, the anisotropic and discontinuous diffusion tensor still exists.

Given the anisotropic diffusion tensor and possible discontinuity across the interface, how to design the accurate discretization for anisotropic diffusion problems have been investigated in the last decades. Finite volume (FV) discretizations of such practical multi-physics problems [41] are very popular due to easy implementation for irregular computational grid and local conservation. As we know, the popular two-point flux approximation (TPFA) has been widely used, nevertheless, its accuracy will degenerate with the presence of anisotropic diffusion tensor. To recover the (second-order) accuracy in the anisotropic case, some finite volume schemes based on more than two points on each side are designed. The pioneer work was proposed in [15], which is the so-called Kershaw scheme. After that, the local support operator scheme (or mimetic finite difference method) [27], nine-point scheme [4, 31], multi-point flux approximation (MPFA) [1] were introduced for the accuracy improvement. Also some variants [8, 10] were proposed for highly anisotropic diffusion tensors. In addition, some nonlinear schemes [28, 23, 36, 38, 43] were proposed for preserving the non-negativity or the discrete maximum principle. However, these traditional numerical schemes have some restrictions on the the mesh distortion and anisotropic diffusion tensor, which limits their application range more or less.

With the advent of the powerful computer and big data, deep neural networks have been extensively used in diverse tasks such as image classification, computer vision, language translation, game intelligence, reservoir parameter inversion [40]. In the context of scientific computing, the idea to use neural network for solving PDEs has been raised since 1990s [19, 17]. Contrast to the traditional mesh-based numerical algorithms, the neural network can be seen as a meshless optimization method. The training process is based on the random sampling strategy. Thus it is less sensitive to the dimensionality of the problems. The high-dimensional PDEs that can not be tackled with traditional mesh-based numerical algorithms are solved by deep neural network [11, 34].

Recently, Raissi et al. [29] developed the so-called physics-informed neural network (PINN) for the solution and discovery of PDEs. the main idea behind the

PINN is that the governing equation is used, rather than the labeled solution, in the loss function to keep the neural network solution approaching the strong solution of PDEs. PINNs have been successfully used in solving a large number of nonlinear PDEs, including Burgers, Schrödinger, Navier-Stokes, Allen-Cahn, high-speed flows, etc [20, 37, 25, 5].

As for the general second-order elliptic problems, the convergence of PINN was studied for linear second-order elliptic and parabolic case firstly in [33] and then in [13] for a quantitative error estimation with respect to the neural networks' depth, width and sampling numbers. Solving a class of second-order boundary-value problems on complex geometries was studied with the penalty manner [2] and penalty-free manner [32]. A class of linear and nonlinear elliptic problems with the unknown diffusion coefficient was considered and learned by the PINN in [35]. In [12], the forward and backward advection-diffusion equations are addressed by PINN, especially for high Péclet number problems. A extreme learning machine with the single hidden layer [6] was proposed for 1D linear advection and diffusion problems. To decrease the order of second-order differential operator and the neural network regularity requirement, the variational PINN was introduced by [16]. Similarly, inspired by the classical mixed finite element method and least-squares finite element method, the deep mixed residual method [24] and first-order deep least-squares methods [3] have been introduced for the general high-order differential PDEs and second-order elliptic PDEs, respectively. The asymptotic preserving first-order deep neural network for the anisotropic elliptic problems was studied in [21]. However, the diffusion equations with the general discontinuous anisotropic tensor are not considered thoroughly in the literature. The anisotropic heat flux across the discontinuous interface is generally discontinuous and so do the solution gradient. The derivatives of these variables near the interface in the loss function will make the training process more difficult. Indeed, as pointed in a recent comprehensive review paper [14], solving PDEs with base PINN indeed may fail in some low-dimensional cases, such as the diffusion equation with non-smooth conductivity.

Therefore, in this paper, we introduce a deep neural network solver based on a new weighted first-order formulation of elliptic anisotropic diffusion problems. More specifically, the original second-order anisotropic diffusion equation is rewritten into a first-order formulation by introducing two auxiliary variables. These auxiliary variables and solution gradient may be discontinuous across the discontinuity interface. The derivative of these variables is not well-defined near the interface pointwisely. A weighted function with the decaying property near the interface is used to multiplied with the first-order formulation, thus the training process will not reinforce a smooth transition nearby the interface and allow to inherit the true jumps of the heat flux. Therefore, the accuracy of the network approximation for the solution is much improved. This is because the anisotropic heat flux is approximated properly in each smooth domain and correctly handled across the discontinuity interfaces.

The remainder of this paper is organized as follows. In Section 2, we will give the

problem setting, a weighted first-order formulation. In Section 3, the deep neural network solver is introduced. In Section 4, we present some numerical results to verify the accuracy improvement. Finally, some conclusions are given in Section 5.

2 A weighted first-order formulation

2.1 The problem setting

We consider the following anisotropic diffusion equation in $\Omega \subset \mathbb{R}^2$:

$$-\nabla \cdot (\Lambda \nabla u) = f \text{ in } \Omega, \quad (2.1)$$

$$u = g \text{ on } \partial\Omega, \quad (2.2)$$

where $\Lambda(x)$ is a 2×2 diffusion tensor, which is a symmetric and positive definite (SPD) function, $g(x)$ is the prescribed boundary condition, and the function $f(x)$ is the so-called source term. If we have $f \geq 0$, $g \geq 0$, then the non-negativity of u is assured by the maximum principle in the continuum setting.

2.2 A weighted first-order formulation

In this section, we will give an equivalent first-order formulation of (2.1) -(2.2).

Let the diffusion tensor $\Lambda(x)$ be

$$\Lambda = \begin{pmatrix} a_{11}(x) & a_{12}(x) \\ a_{12}(x) & a_{22}(x) \end{pmatrix}.$$

In the sequel, we will omit the space-dependence on x of each component a_{ij} of Λ . Based on the elementary linear algebra, the eigenvalues of Λ are

$$\begin{aligned} \lambda_1 &= \frac{a_{11} + a_{22} + \sqrt{(a_{11} - a_{22})^2 + 4a_{12}^2}}{2}, \\ \lambda_2 &= \frac{a_{11} + a_{22} - \sqrt{(a_{11} - a_{22})^2 + 4a_{12}^2}}{2}. \end{aligned}$$

With the two eigenvalues, we have two orthogonal eigenvectors as

$$\begin{aligned} \hat{q}_1 &= (-a_{12}, \lambda_2 - a_{22})^T, \\ \hat{q}_2 &= (\lambda_1 - a_{11}, -a_{12})^T. \end{aligned}$$

Then the unit eigenvectors are given as

$$q_1 = \frac{\hat{q}_1}{\|\hat{q}_1\|},$$

$$q_2 = \frac{\hat{q}_2}{\|\hat{q}_2\|}.$$

With these two unit eigenvectors, we can decompose the heat flux $q = \Lambda \nabla u$ as

$$q = (\Lambda \nabla u, q_1)q_1 + (\Lambda \nabla u, q_2)q_2.$$

Moreover, we define two auxiliary variables as

$$\begin{aligned} \tau &= (\Lambda \nabla u, q_1), \\ \phi &= (\Lambda \nabla u, q_2), \end{aligned}$$

then we have a first-order formulation equivalent to (2.1) -(2.2)

$$\begin{cases} -\nabla \cdot (\tau q_1 + \phi q_2) = f, & \text{in } \Omega, \\ \tau = (\Lambda \nabla u, q_1), & \text{in } \Omega, \\ \phi = (\Lambda \nabla u, q_2), & \text{in } \Omega, \\ u = g, & \text{on } \partial\Omega. \end{cases} \quad (2.3)$$

Given that the diffusion tensor Λ may have the discontinuity across the interface, the exact solution gradient ∇u and two variables (τ, ϕ) may be discontinuous. The point-wise definition in PINN may be ill-posed in the points nearby the interface. Namely, more points sampled in this region, will cause the derivative of those discontinuous variables become more larger, so do the loss function. Thus the larger dispersion of these variables will appear for making the loss function decreased. The resulted neural network approximation will deviate the true solution profile. To relieve this deviation, we define the distance-weighted function $\zeta(x)$ in the whole domain. The function $\zeta(x)$ will approach to zero when x is approaching to the interface, and be $O(1)$ in the other domains. For convenience, we define the transition

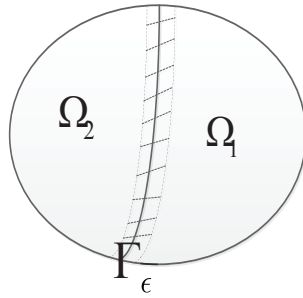


Figure 1: The jumping interface transition region Γ_ϵ .

domain for each interface Γ as

$$\Gamma_\epsilon = \{x \in \Omega, \text{dist}(x, \Gamma) \leq \epsilon\},$$

then

$$\zeta(x) = \begin{cases} \frac{\text{dist}(x, \Gamma^i)}{\text{dist}(x, \Gamma^i) + \epsilon}, & \text{in } \Gamma_\epsilon^i, \\ \frac{1}{2}, & \text{in } \Omega \setminus \cup_i \Gamma_\epsilon^i, \end{cases} \quad (2.4)$$

where ϵ is the pre-defined parameter of transition width. For example, the domain occupies one diffusion tensor discontinuity interface Γ as in Fig. 1, then the transition domain Γ_ϵ is the shadow domain, and $\zeta(x) = \frac{\text{dist}(x, \Gamma)}{\text{dist}(x, \Gamma) + \epsilon}$ in this region, equal to $\frac{1}{2}$ otherwise.

With the help of function $\zeta(x)$, we have a new weighted first-order formulation as

$$\begin{cases} \zeta(f + \nabla \cdot (\tau q_1 + \phi q_2)) = 0, & \text{in } \Omega, \\ \zeta(\tau - (\Lambda \nabla u, q_1)) = 0, & \text{in } \Omega, \\ \zeta(\phi - (\Lambda \nabla u, q_2)) = 0, & \text{in } \Omega, \\ u = g, & \text{on } \partial\Omega. \end{cases} \quad (2.5)$$

Remark 2.1. For 3D anisotropic case, three orthogonal eigenvectors (q_1, q_2, q_3) are also available and can be used to define three auxiliary variables (τ, ϕ, ψ). The similar distance-weighted function ζ should be applied. In 2D/3D isotropic case, we just choose $q_i = e_i$, which is the unit elementary basis in cartesian coordinates, and the width of transition domain can be chosen as the machine precision.

3 Deep neural network solver

3.1 Deep neural network architecture

We will briefly introduce the deep neural network structure used in this paper. Generally, a deep neural network defines a nonlinear function

$$\mathcal{N} : \mathbf{x} \in \mathbb{R}^d \rightarrow \mathbf{y} \in \mathbb{R}^c,$$

where d and c are the dimensions of the input and output, respectively. $\mathcal{N}(\mathbf{x})$ is a composite function of some different layers of functions as

$$\mathcal{N}(\mathbf{x}) = \mathcal{N}^{(L)} \circ \dots \circ \mathcal{N}^{(2)} \circ \mathcal{N}^{(1)}(\mathbf{x}),$$

where L is the number of layers or the so-called depth of the neural network (see Fig. 2).

For the k th layer $\mathcal{N}^{(k)}$, we use full connected hidden layers, that is,

$$\mathcal{N}^{(k)}(\mathbf{x}^{k-1}) = \sigma(W^k \mathbf{x}^{k-1} + b^k), \quad 1 \leq k < L,$$

$$\mathcal{N}^{(L)}(\mathbf{x}^{L-1}) = W^L \mathbf{x}^{L-1} + b^L, \quad k = L,$$

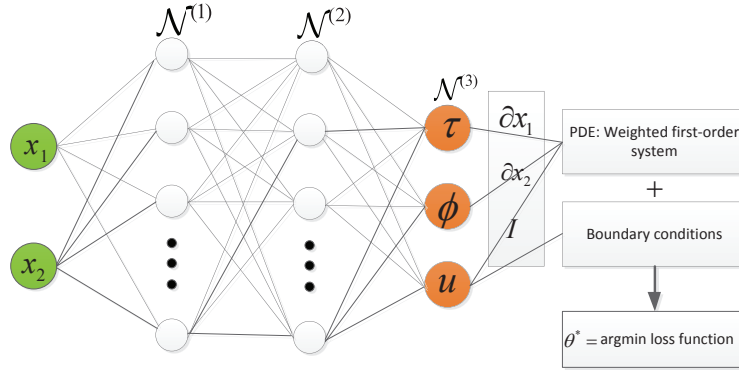


Figure 2: The network structure ($L = 3$), the output is then evaluated with automatic differentiation to get the PDE residual and boundary condition residual.

where n_k is the width of k th layer, the matrix $W^k \in \mathbb{R}^{n_k \times n_{k-1}}$ and vector $b^k \in \mathbb{R}^{n_k}$ are called the weights and bias, respectively. All the weights and bias are denoted as $\theta = \{(W^k, b^k)\}_{k=1, \dots, L}$, which are the parameters to be trained. The function σ is generally nonlinear and called the activation function. Several classical activation functions are ReLU function, sigmoid function, hyperbolic tangent function, etc. In this paper, the hyperbolic tangent function is used as the activation function (see Fig. 3)

$$\sigma(\mathbf{x}) = \tanh(\mathbf{x}),$$

where it is applied component-wisely. With this activation function and multiple hidden layers, the deep neural network can approximate a large class of complex nonlinear function rather than the linear ones.

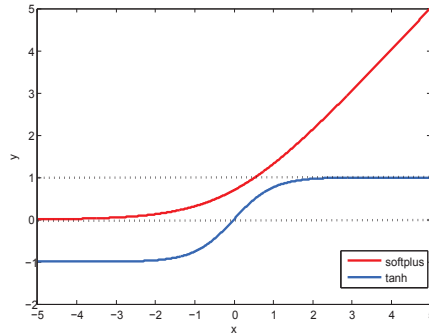


Figure 3: The activation function and softplus function.

3.2 The discrete least-squares functional

In this part, the least-squares formulation for the first-order weighted formulation (2.5) is given, then the discrete version based on the deep neural network approxi-

mation is introduced.

The first-order weighted least-squares formulation is to find $(u, \tau, \phi) \in (H^1(\Omega))^3$ such that

$$\Psi(u, \tau, \phi; \mathbf{f}) = \min_{(\eta, \nu, \chi) \in (H^1(\Omega))^3} \Psi(\eta, \nu, \chi; \mathbf{f}), \quad (3.1)$$

where $\mathbf{f} = (f, g, \zeta)$ and

$$\begin{aligned} \Psi(\eta, \nu, \chi; \mathbf{f}) &= \|\zeta(f + \nabla \cdot (\nu q_1 + \chi q_2))\|_{0,\Omega}^2 + \|\zeta(\nu - (\Lambda \nabla \eta, q_1))\|_{0,\Omega}^2 \\ &\quad + \|\zeta(\chi - (\Lambda \nabla \eta, q_2))\|_{0,\Omega}^2 + \|\eta - g\|_{1/2,\partial\Omega}^2. \end{aligned} \quad (3.2)$$

If three unknown functions u, τ, ϕ are approximated by one deep neural network and its three outputs are denoted by $\hat{u}(x, \theta), \hat{\tau}(x, \theta), \hat{\phi}(x, \theta)$ (see Fig. 2), then the discrete formulation based on all sampling points reads

$$\hat{\Psi}(\hat{u}, \hat{\tau}, \hat{\phi}; \mathbf{f})(\theta) = \min_{\tilde{\theta} \in \mathbb{R}^N} \hat{\Psi}(\hat{\eta}, \hat{\nu}, \hat{\chi}; \mathbf{f})(\tilde{\theta}), \quad (3.3)$$

where the discrete functional reads

$$\begin{aligned} \hat{\Psi}(\hat{\eta}, \hat{\nu}, \hat{\chi}; \mathbf{f})(\tilde{\theta}) &= \frac{1}{N_f} \sum_{i=1}^{N_f} (\zeta(\mathbf{x}_i)(f(\mathbf{x}_i) + \nabla \cdot (\hat{\nu}(\mathbf{x}_i, \tilde{\theta})q_1(\mathbf{x}_i) + \hat{\chi}(\mathbf{x}_i, \tilde{\theta})q_2(\mathbf{x}_i)))^2 \\ &\quad + \frac{1}{N_f} \sum_{i=1}^{N_f} (\zeta(\mathbf{x}_i)(\hat{\nu}(\mathbf{x}_i, \tilde{\theta}) - (\Lambda \nabla \hat{\eta}(\mathbf{x}_i, \tilde{\theta}), q_1(\mathbf{x}_i)))^2 \\ &\quad + \frac{1}{N_f} \sum_{i=1}^{N_f} (\zeta(\mathbf{x}_i)(\hat{\chi}(\mathbf{x}_i, \tilde{\theta}) - (\Lambda \nabla \hat{\eta}(\mathbf{x}_i, \tilde{\theta}), q_2(\mathbf{x}_i)))^2 \\ &\quad + \frac{\omega_D}{N_D} \sum_{i=1}^{N_D} (\hat{\eta}(\mathbf{x}_i, \tilde{\theta}) - g(\mathbf{x}_i))^2, \end{aligned} \quad (3.4)$$

where N_f, N_D are number of collocation points in Ω and on $\partial\Omega$, the total number of network parameters is $N = \sum_{i=1}^L n_i(n_{i-1} + 1)$ and ω_D represents the boundary-weight to penalize the neural network approximations satisfying the boundary conditions.

Remark 3.1. *As pointed in deep mixed residual method [24] and deep least-squares method [3], the three unknown functions can also employ more than one neural network (multiple different neural networks) to approximate them. This may offer another flexibility and accuracy improvement for solving this weighted first-order system.*

Remark 3.2. *In some cases, if the function $\mathbf{f} \geq 0$, the analytical solution u is non-negative by the maximum principle. To enforce this constraints, two alternative ways*

are possible. One is the penalty way similar to the boundary condition enforcement reads

$$\hat{\Psi}_{p_1}(\hat{\eta}, \hat{\nu}, \hat{\chi}; \mathbf{f})(\tilde{\theta}) = \hat{\Psi}(\hat{\eta}, \hat{\nu}, \hat{\chi}; \mathbf{f})(\tilde{\theta}) + \frac{\omega_{p_1}}{N_f} \sum_{i=1}^{N_f} \max(-u(\mathbf{x}_i, \tilde{\theta}), 0)^2,$$

where ω_{p_1} is the penalty parameter. Another way is to apply the softplus function $\ln(1 + e^x)$ (see Fig. 3) to the network output $\hat{\eta}$ as $\bar{\eta} = \ln(1 + e^{\hat{\eta}})$, then the discrete functional is replaced as

$$\hat{\Psi}_{p_2}(\bar{\eta}, \hat{\nu}, \hat{\chi}; \mathbf{f})(\tilde{\theta}) = \hat{\Psi}(\bar{\eta}, \hat{\nu}, \hat{\chi}; \mathbf{f})(\tilde{\theta}),$$

and then the final neural network approximation becomes (\bar{u}, τ, ϕ) with $\bar{u} \geq 0$ almost everywhere.

Remark 3.3. For completeness and comparison, we also give the base PINN discrete formulation for the anisotropic diffusion problems as follows

$$\hat{\Psi}_{PINN}(\hat{u}; \mathbf{f}_1)(\theta) = \min_{\tilde{\theta} \in \mathbb{R}^N} \hat{\Psi}_{PINN}(\hat{\eta}; \mathbf{f}_1)(\tilde{\theta}), \quad (3.5)$$

where the discrete functional reads

$$\begin{aligned} \hat{\Psi}_{PINN}(\hat{\eta}; \mathbf{f}_1)(\tilde{\theta}) &= \frac{1}{N_f} \sum_{i=1}^{N_f} ((f(\mathbf{x}_i) + \nabla \cdot (\Lambda(\mathbf{x}_i) \nabla \hat{\eta}(\mathbf{x}_i, \tilde{\theta})))^2 \\ &+ \frac{\omega_D}{N_D} \sum_{i=1}^{N_D} (\hat{\eta}(\mathbf{x}_i, \tilde{\theta}) - g(\mathbf{x}_i))^2, \end{aligned} \quad (3.6)$$

where $\mathbf{f}_1 = (f, g)$, N_f , N_D are number of collocation points in Ω and on $\partial\Omega$, and ω_D represents the boundary-weight to penalize the neural network approximations satisfying the boundary conditions.

4 Numerical results

In this section, we test several diffusion problems with continuous or discontinuous anisotropic diffusion tensors. For simplicity, our method is denoted as weighted FO-PINN. For both base PINN and our weighted FO-PINN, we use the same neural network structure. More specifically, we use a five-layer neural network with 16 neurons to approximate the solution u and two auxiliary variables simultaneously in our method, and a five-layer neural network with 16 neurons just for the solution approximation in base PINN method. The activation function for all hidden layers is the tanh function and identity for the last output layer.

If there exists the analytical solution, we use the following relative discrete L_2 -norm to evaluate the accuracy of learned solution

$$\epsilon_2^u = \frac{\|u - u_e\|_2}{\|u_e\|_2},$$

where u_e is the problem-dependent analytical solution.

To implement and train the neural network, an integrated Python software deep-XDE [20] based TensorFlow is used to implement the base PINN and our method. To train the neural network parameters θ efficiently, the Adam optimizer version of gradient descent is used with a pre-defined number of iterations, then the L-BFGS-B optimizer is used for achieving the final convergence. The learning rate is initialized as $1e-3$ and will decrease gradually as the iteration steps growing. The collocation points are sampled randomly from the interior domain and domain boundary with the specific numbers N_f and N_D .

4.1 The diffusion problem with smooth anisotropic coefficient

We first test the accuracy for diffusion problem with smooth anisotropic coefficients. Consider the problem (2.1) with Dirichlet boundary condition in the unit square $\Omega = (0, 1)^2$. The exact analytical solution and the diffusion coefficient coming from the FVCA6 benchmark [9] are $u = 1 + \sin(2\pi x) \sin(2\pi y)$ and

$$\Lambda = \begin{bmatrix} 1 & \\ & 10^3 \end{bmatrix}.$$

The source f and the Dirichlet boundary data g are set accordingly to the exact solution.

In this case, we use $N_f = 10000$ collocation points, $N_D = 1000$ boundary points and boundary-weight $\omega_D = 100$, the Adam optimizer is used until 10000 iterations and then L-BFGS-B optimizer is used to reach convergence.

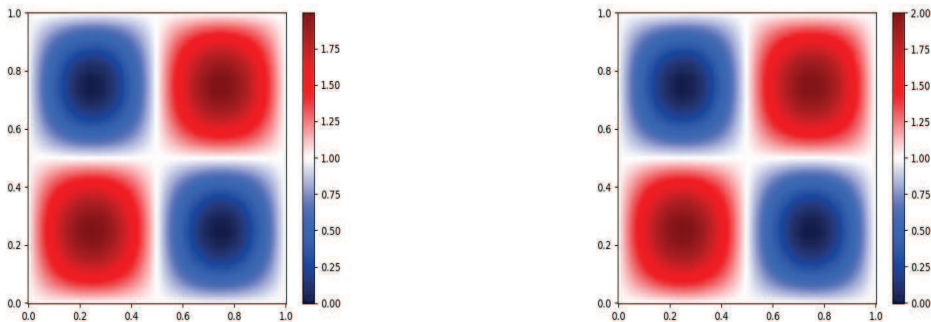


Figure 4: The solution profiles of base PINN (left) and weighted FO-PINN (right).

The numerical results for base PINN and our weighted FO-PINN are shown in Fig. 4. The discrete relative L_2 -norm for base PINN and weighted FO-PINN are

2.93e-3 and 4.1e-3, respectively. We can see that both methods are quite accurate for this smooth problem, and our method can naturally solve this problem by setting the weight function ζ equal to 1/2 in the whole domain.

4.2 The diffusion problem with discontinuous isotropic coefficient

Next, we consider the problem (2.1-2.2) with Dirichlet boundary condition in the unit domain $\Omega = [0, 1]^2$. The diffusion tensor $\Lambda(x)$ is a isotropic but discontinuous tensor and given by

$$\Lambda = \begin{cases} 5, & x \leq 0.5, \\ 1, & x > 0.5. \end{cases}$$

The analytical solution is chosen to be

$$u = \begin{cases} (x^2 + 10)(y - y^2), & x \leq 0.5, \\ (5x^2 + 9)(y - y^2), & x > 0.5. \end{cases}$$

The source f and the Dirichlet boundary data g are set accordingly to the exact solution.

In this case, we use $N_f = 10000$ collocation points, $N_D = 2000$ boundary points, and the interior weights and boundary-weight are chosen as the inverse of the initial losses of each term such that the weighted losses are of the same order of magnitude $O(1)$, the Adam optimizer is used until 10000 iterations and then L-BFGS-B optimizer is used to reach convergence.

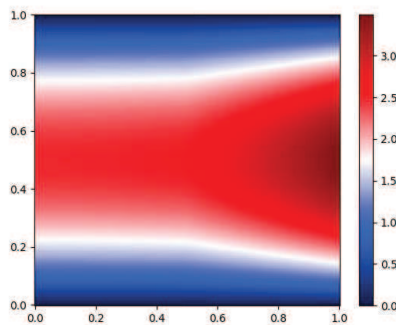


Figure 5: The exact solution profile for isotropic but discontinuous diffusion tensor.

The exact solution is depicted in Fig. 5 for comparison. The numerical results for base PINN and our weighted FO-PINN are shown in Fig. 6. The discrete relative L_2 -norm for base PINN and weighted FO-PINN are $2.64e-2$ and $8.06e-3$, respectively. We can see that our method is more accurate than the base PINN

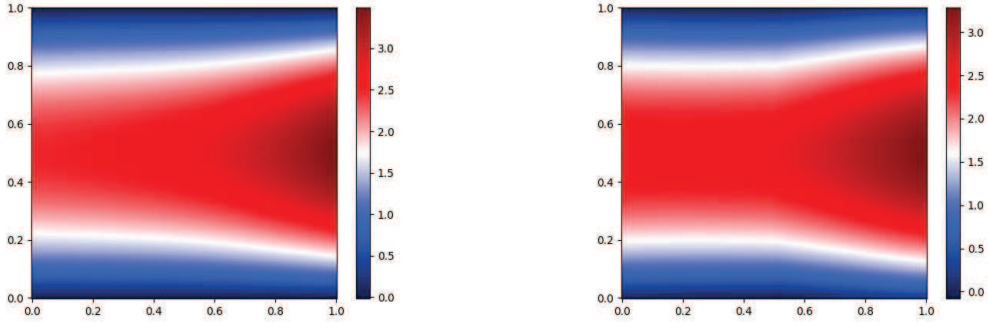


Figure 6: The solution profiles of base PINN (left) and weighted FO-PINN (right).

method for this discontinuous isotropic case, and the transition region width ϵ in the weighted function ζ is equal to 0.01. It is shown that the resolution of our method is higher with the curved contours near the discontinuous interface.

4.3 The diffusion problem with discontinuous anisotropic coefficient

In this subsection, we demonstrate the accuracy for diffusion problem with the discontinuous and mild anisotropic coefficient, where many traditional cell-centered finite volume schemes also will undergo the accuracy degeneracy. Let the exact solution and the diffusion coefficient be as follows:

$$\Lambda = \begin{cases} \begin{pmatrix} 1 & 0 \\ 0 & 1 \end{pmatrix}, & x \leq 0.5, \\ \begin{pmatrix} 10 & 3 \\ 3 & 1 \end{pmatrix}, & x > 0.5, \end{cases}$$

and the analytical solution is chosen to be

$$u(x, y) = \begin{cases} -2y^2 + 4xy + 6x + 2y + 1, & x \leq 0.5, \\ -2y^2 + 1.6xy - 0.6x + 3.2y + 4.3, & x > 0.5. \end{cases}$$

The source term and Dirichlet boundary condition are computed by this analytical solution.

In this case, we use the same neural network structure as the last one. The number of collocation points and optimization method for training are also the same as it. The exact solution and the solution of base PINN method are depicted in Fig. 7 for comparison. We can see that the base PINN can not capture the correct heat flux even in one-side domain. As shown in Fig. 8 (left), the pure first-order formulation is better for capturing the heat flux in one-side domain, but is less accurate across the jump interface. By adding the weighted function ζ with transition width $\epsilon = 0.01$,

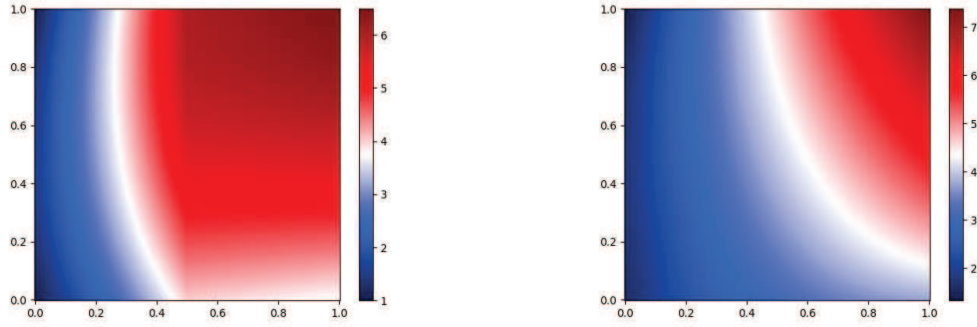


Figure 7: The exact solution profile (left) and the solution profile of base PINN (right).

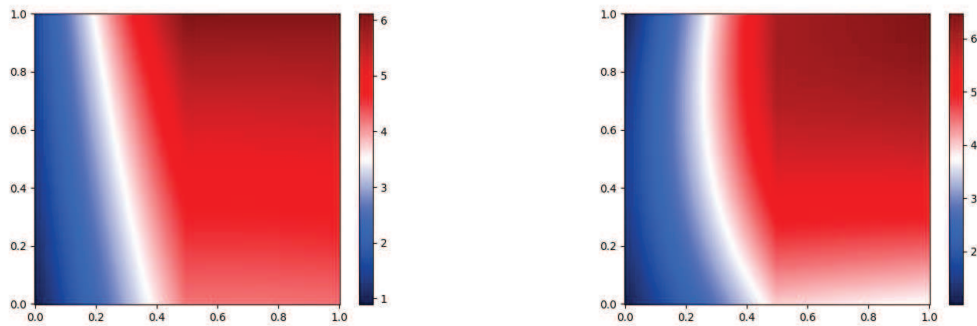


Figure 8: The solution profiles of pure FO-PINN (left) and weighted FO-PINN (right).

The numerical result for the weighted FO-PINN is shown in Fig. 8 (right), whose solution profile is closest to the exact solution. The discrete relative L_2 -norms for base PINN, pure FO-PINN and weighted FO-PINN are $1.42e - 1$, $7.18e - 2$ and $6.31e - 3$, respectively. We can see that our method is much more accurate than the base PINN method for this discontinuous anisotropic case, and the weighted function ζ is crucial for the resolution near the discontinuous interface and approximation of the heat flux across the interface.

To test the accuracy and efficiency of our method in higher dimension, we consider a similar 3D case as follows:

$$\Lambda = \begin{cases} \begin{pmatrix} 1 & 0 & 0 \\ 0 & 1 & 0 \\ 0 & 0 & 1 \end{pmatrix}, & x \leq 0.5, \\ \begin{pmatrix} 10 & 3 & 0 \\ 3 & 1 & 0 \\ 0 & 0 & 1 \end{pmatrix}, & x > 0.5, \end{cases}$$

and the analytical solution is chosen to be

$$u(x, y, z) = \begin{cases} -2y^2 + 4xy + 6x + 2y + z + 1, & x \leq 0.5, \\ -2y^2 + 1.6xy - 0.6x + 3.2y + z + 4.3, & x > 0.5. \end{cases}$$

The source term and Dirichlet boundary condition are computed by this analytical solution.

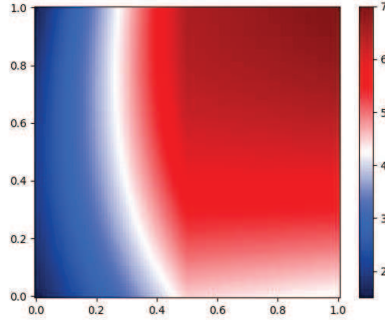


Figure 9: The exact solution slide on $z = 0.5$ plane for 3D discontinuous diffusion tensor.

In this case, the same neural network structure as 2D case is used, only the number of outputs is different. We choose $N_f = 20000$ collocation points and $N_D = 2000$ boundary points as twice as 2D counterparts. The exact solution slide on $z = 0.5$ plane is depicted in Fig. 9 for comparison. The numerical results for base PINN and our weighted FO-PINN are shown in Fig. 10. The discrete relative L_2 -norm for base PINN and weighted FO-PINN are $1.19e - 1$ and $2.67e - 3$, respectively. We

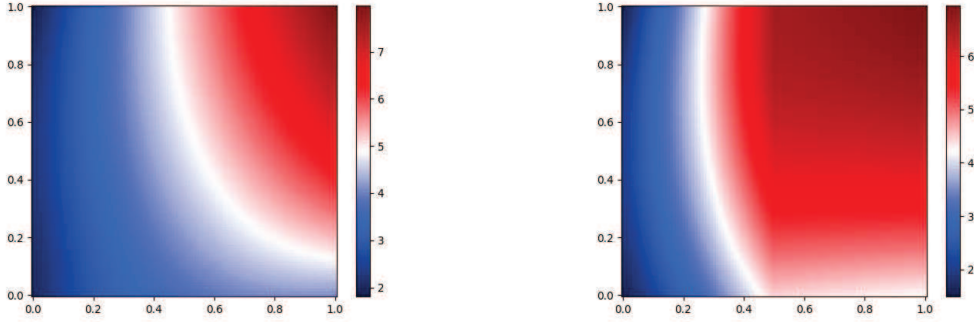


Figure 10: The 3D solution slide on $z = 0.5$ plane of base PINN (left) and weighted FO-PINN (right).

can see that our method is also more accurate than the base PINN method for this 3D anisotropic case, and the accuracy of base PINN is slightly worse than 2D, while ours is more accurate than 2D counterpart. It is shown that our neural network approximation is less sensitive to the dimensionality.

4.4 The diffusion problem with strong anisotropic coefficient

In this subsection, we demonstrate the accuracy for diffusion problem with a strong anisotropic diffusion coefficient with more discontinuities. This example is modified from [8], such that the gradient of the solution has discontinuity across the interfaces. The domain $\Omega = [0, 1]^2$ is split into four subdomains $\Omega = \bigcup_{i=1}^4 \Omega_i$, which are given by

$$\begin{aligned}
 \Omega_1 &= \{(x, y) \in [0, 1]^2 \text{ such that } x \leq 0.5, y \leq 0.5\} \\
 \Omega_2 &= \{(x, y) \in [0, 1]^2 \text{ such that } x > 0.5, y \leq 0.5\} \\
 \Omega_3 &= \{(x, y) \in [0, 1]^2 \text{ such that } x > 0.5, y > 0.5\} \\
 \Omega_4 &= \{(x, y) \in [0, 1]^2 \text{ such that } x \leq 0.5, y > 0.5\}
 \end{aligned}$$

The diffusion coefficient and the exact solution are given by

$$\Lambda = \begin{bmatrix} a_x^i & 0 \\ 0 & a_y^i \end{bmatrix}, \text{ for } (x, y) \in \Omega_i, \text{ with }$$

i	1	2	3	4
a_x^i	10	0.1	0.01	100
a_y^i	0.01	100	10	0.1
α_i	0.1	10	100	0.01

and

$$u(x, y) = \alpha_i \sin(2\pi x) \sin(2\pi y).$$

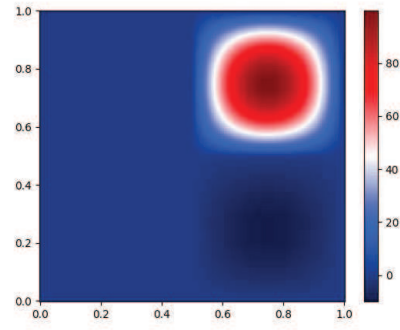


Figure 11: The exact solution profile for strong discontinuous diffusion tensor.

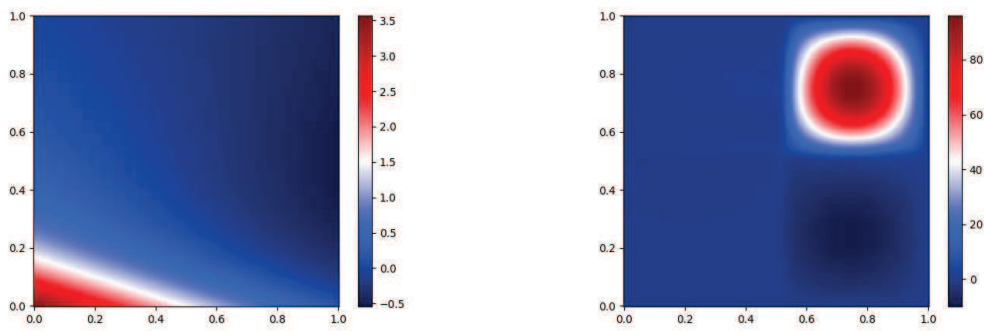


Figure 12: The solution profiles of base PINN (left) and weighted FO-PINN (right).

In this case, we use the same neural network structure as the last one. The number of collocation points and optimization method for training are also the same as it. The exact solution are depicted in Fig. 11 for comparison. As shown in Fig. 12 (left), the base PINN is failed to capture the solution profile, while our weighted FO-PINN is quite close to the true solution, see Fig. 12 (right). The discrete relative L_2 -norms for base PINN and weighted FO-PINN are $1.01e-0$ and $6.90e-2$, respectively. We can see that our method is much more accurate than the base PINN method for this strong discontinuous anisotropic case, and the weighted function ζ with parameter $\epsilon = 0.01$ is used for the resolution near the discontinuous interface and approximation of the heat flux across the internal interfaces.

4.5 Anisotropic diffusion problems with local source term

Let us consider the steady problem (2.1-2.2) with the local source term in the unit domain $\Omega = [0, 1]^2$ and set

$$\Lambda = \begin{pmatrix} \cos \theta & \sin \theta \\ -\sin \theta & \cos \theta \end{pmatrix} \begin{pmatrix} k_1 & 0 \\ 0 & k_2 \end{pmatrix} \begin{pmatrix} \cos \theta & -\sin \theta \\ \sin \theta & \cos \theta \end{pmatrix}$$

and

$$f = \begin{cases} 1000 & \text{if } (x, y, z) \in [7/18, 11/18]^2, \\ 0 & \text{otherwise,} \end{cases}$$

where $\theta = \pi/6$, $(k_1, k_2) = (1, 1000)$. The boundary condition $g = 0$ is imposed.

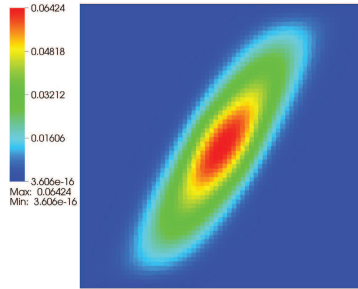


Figure 13: The numerical solution profile with monotone finite volume scheme [39].

Although there is no analytical solution, for comparison, we give the reference solution computed with the monotone finite volume scheme [39] in Fig. 13. As shown in Fig. 14 (left), the solution of base PINN has more oscillations, and the heat flux is not mainly along the rotated vector $(\sin \frac{\pi}{6}, \cos \frac{\pi}{6})^T$. while the solution of our weighted FO-PINN is much less oscillated, quite close to the reference solution,

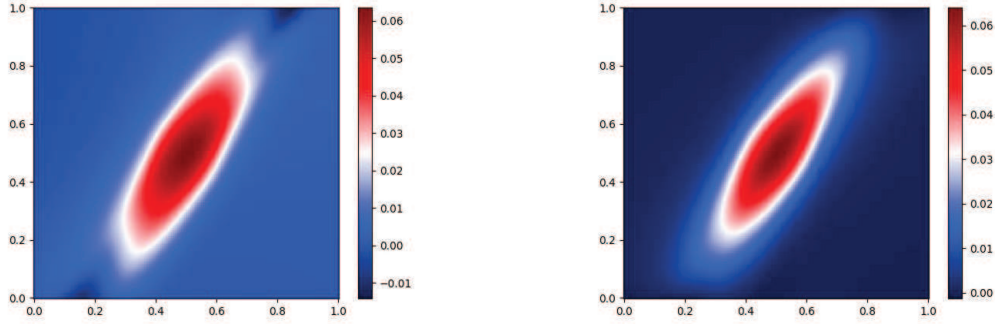


Figure 14: The solution profiles of base PINN (left) and weighted FO-PINN (right).

and the heat flux is mainly along the direction of the above rotated vector. It is shown that our method is more accurate than the base PINN for this rotated anisotropic diffusion problem.

Let us consider another steady problem (2.1-2.2) with local source term in the unit domain $\Omega = [0, 1]^2$ and set

$$\Lambda = \begin{pmatrix} \epsilon_1 x^2 + y^2 & (\epsilon_1 - 1)xy \\ (\epsilon_1 - 1)xy & x^2 + \epsilon_1 y^2 \end{pmatrix}, \quad \epsilon_1 = 5.0e - 3,$$

and

$$f = \begin{cases} 1 & \text{if } (x, y) \in [3/8, 5/8]^2, \\ 0 & \text{otherwise.} \end{cases}$$

The homogeneous boundary condition $g = 0$ is imposed.

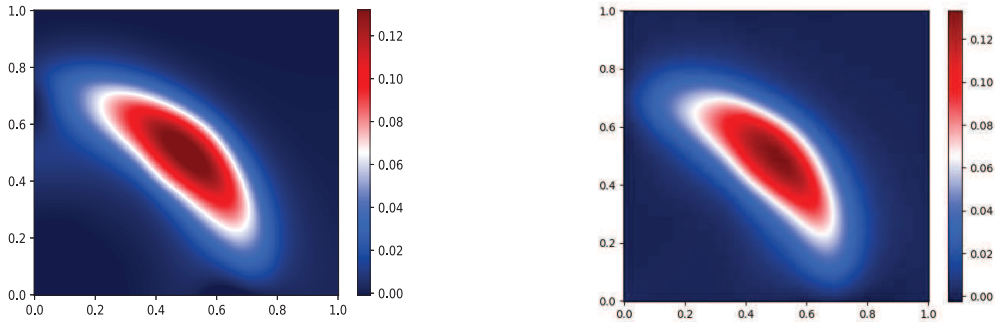


Figure 15: The solution profiles of base PINN (left) and weighted FO-PINN (right).

With this case, we will show our method can deal with the diffusion tensor whose eigenvectors are space-dependent. As shown in Fig. 15, the solution distribution of base PINN and our weighted FO-PINN are similar. However, compared with

the numerical results in [42], the maximum solution value of our method is more close to the one in the literature. It is shown that our method is accurate for this space-dependent anisotropic diffusion problem and the accuracy is comparable to some traditional numerical schemes.

Conclusions

A new weighted first-order formulation is proposed for solving the anisotropic diffusion problems with deep neural networks. The weighted first-order formulation is first obtained by introducing two components of the heat flux along the eigenvectors of the anisotropic diffusion tensor. Then the possible discontinuity of the heat flux across the interface is correctly approximated by multiplying the first-order formulation with the decaying weighted function. By various numerical examples, we can see that the smooth diffusion problem can be solved with setting the transition width to machine precision, and by setting a proper transition width ($\epsilon = 0.01$ by our empirical experience) for the discontinuous interface, the numerical accuracy for the discontinuous anisotropic diffusion problems is much improved, while the algorithm efficiency is comparable with the base PINN due to the same neural network structure is employed. In addition, the 3D test shows that our method does not suffer from the curse of dimensionality as much as other numerical schemes.

Acknowledgements

This work was partially supported by the National Natural Science Foundation of China (No. 11901043).

References

- [1] I. Aavatsmark, An introduction to multipoint flux approximations for quadrilateral grids, *Comput. Geosci.*, 6 (2002), 405–432.
- [2] J. Berg, K. Nystrom, A unified deep artificial neural network approach to partial differential equations in complex geometries, *Neurocomputing*, 317 (2018), 28–41.
- [3] Z. Cai, J. Chen, M. Liu, et al., Deep least-squares methods: An unsupervised learning-based numerical method for solving elliptic PDEs, *J. Comput. Phys.*, 420(2020), 109707.

- [4] G. Chen, D. Li, Z. Su, Difference scheme by integral interpolation method for three dimensional diffusion equations , Chinese J. Comput. Phys., 20(2003), 205–209.
- [5] S. Cuomo, V. S. D. Cola, F. Giampaolo, et al., Scientific machine learning through physics-informed neural networks: where we are and what’s next , (2022), arXiv: 2201.05624v3.
- [6] V. Dwivedi, B. Srinivasan, Physics informed extreme learning machine (PIELM)- A rapid method for the numerical solution of partial differential equations, Neurocomputing, 391 (2020), 96–118.
- [7] J. Droniou, Finite volume schemes for diffusion equations: introduction to and review of modern methods, Math. Models Methods Appl. Sci.(M3AS), 24 (2014), 1575–1619.
- [8] M. G. Edwards, H. Zheng, Quasi M-matrix multifamily continuous Darcy-flux approximations with full pressure support on structured and unstructured grids in three dimensions, SIAM J. Sci. Comput., 33 (2011), 455–487.
- [9] R. Eymard, G. Henry, R. Herbin, et al., 3D benchmark on discretization schemes for anisotropic diffusion problems on general grids, in: Finite Volumes for Complex Applications VI Problems and Perspectives, (2011), 895–930.
- [10] Z. Gao, J. Wu, A linearity-preserving cell-centered scheme for the heterogeneous and anisotropic diffusion equations on general meshes, Int. J. Numer. Meth. Fluids, 67 (2011), 2157–2183.
- [11] J. Han, A. Jentzen, Weinan E., Solving high-dimensional partial differential equations using deep learning, Proc. Natl. Acad. Sci. Unit. States Am., 115(2018), 8505–8510.
- [12] Q. He, A. M. Tartakovsky, Physics-informed neural network method for forward and backward advection-dispersion equations, Water Resour. Res., 57(7)(2021), e2020WR029479.
- [13] Y. Jiao, Y. Lai, D. Li, et al., A rate of convergence of physics informed neural networks for the linear second order elliptic PDEs, Commun. Comput. Phys., 31(4)(2022), 1272–1295.
- [14] G. E. Karniadakis, I. G. Kevrekidis, L. Lu, et al., Physics-informed machine learning, Nat. Rev. Phys., 3 (2021), 422–440.
- [15] D. S. Kershaw, Differencing of the diffusion equation in Lagrangian hydrodynamic codes, J. Comput. Phys., 39 (1981), 375–395.

- [16] E. Kharazmi, Z. Zhang, G. E. Karniadakis, Variational physics-informed neural networks for solving partial differential equations, (2019), arXiv: 1912.00873.
- [17] I. E. Lagaris, A. Likas, D. I. Fotiadis, Artificial neural networks for solving ordinary and partial differential equations, *IEEE Trans. Neural Netw.*, 9 (1998), 987–1000.
- [18] K. Lan, J. Liu, Z. Li, et al., Progress in octahedral spherical hohlraum study, *Matter Radiat. Extrem.*, 1 (2016), 8–27.
- [19] H. Lee, I. S. Kang, Neural algorithms for solving differential equations, *J. Comput. Phys.*, 91 (1990), 110–131.
- [20] L. Lu, X. Meng, Z. Mao, G. E. Karniadakis, DeepXDE: a deep learning library for solving differential equations, *SIAM Rev.*, 63 (2021), 208–228.
- [21] L. Li, C. Yang, APFOS-NET: Asymptotic preserving scheme for anisotropic elliptic equations with deep neural network, *J. Comput. Phys.*, 453 (2022), 110958.
- [22] J. Lindl, Development of the indirect-drive approach to inertial confinement fusion and the target physics basis for ignition and gain, *Phys. Plasmas*, 2 (1995), 3933–4023.
- [23] K. Lipnikov, M. Shashkov, D. Svyatskiy, Y. Vassilevski, Monotone finite volume schemes for diffusion equations on unstructured triangular and shape-regular polygonal meshes, *J. Comput. Phys.*, 227 (2007), 492–512.
- [24] L. Lyu, Z. Zhang, M. Chen, et al., MIM: a deep mixed residual method for solving high-order partial differential equations, *J. Comput. Phys.*, 452 (2022), 110930.
- [25] Z. Mao, A. D. Jagtap, G. E. Karniadakis, Physics-informed neural networks for high-speed flows, *Comput. Methods Appl. Mech. Engrg.*, 360 (2020), 112789.
- [26] C. D. Meyer, D. S. Balsara, T. D. Aslam, A second-order accurate Super TimeStepping formulation for anisotropic thermal conduction, *Mon. Not. R. Astron. Soc.*, 422 (2012), 2102–2115.
- [27] J. Morel, J. Dendy, M. Hall, and S. White, A cell-centered Lagrangian-mesh diffusion differencing scheme, *J. Comput. Phys.*, 103 (1992), 286–299.
- [28] C. Le Potier, Finite volume monotone scheme for highly anisotropic diffusion operators on unstructured triangular meshes, *C. R. Acad. Sci. Paris, Ser. I*, 341 (2005), 787–792.

- [29] M. Raissi, P. Perdikaris, G. E. Karniadakis, Physics-informed neural networks: a deep learning framework for solving forward and inverse problems involving nonlinear partial differential equations, *J. Comput. Phys.*, 378 (2019), 686–707.
- [30] M. Schneider, B. Flemisch, R. Helmig, K. Terekhov, H. Tchelepi, Monotone nonlinear finite-volume method for challenging grids, *Comput. Geosci.*, 22(2) (2018), 565–586.
- [31] Z. Sheng, G. Yuan, A nine point scheme for the approximation of diffusion operators on distorted quadrilateral meshes, *SIAM J. Sci. Comput.*, 30 (2008), 1341–1361.
- [32] H. Sheng, C. Yang, PFNN: a penalty-free neural network method for solving a class of second-order boundary-value problems on complex geometries, *J. Comput. Phys.*, 428 (2021), 110085.
- [33] Y. Shin, J. Darbon, G. E. Karniadakis, On the convergence of physics informed neural networks for linear second-order elliptic and parabolic type PDEs, *Commun. Comput. Phys.*, 28 (2020), 2042–2074.
- [34] J. Sirignano, K. Spiliopoulos, DGM: a deep learning algorithms for solving partial differential equations, *J. Comput. Phys.*, 375(2018), 1339–1364.
- [35] A. M. Tartakovsky, C. O. Marrero, P. Perdikaris, et al., Physics-informed deep neural networks for learning parameters and constitute relationship in subsurface flow problems, *Water Resour. Res.*, 56(5) (2020), e2019ER026731.
- [36] K. M. Terekhov, B. T. Mallison, H. A. Tchelepi, Cell-centered nonlinear finite volume methods for the heterogeneous anisotropic diffusion problem, *J. Comput. Phys.*, 330 (2017), 245–267.
- [37] C. L. Wight, J. Zhao, Solving Allen-Cahn and Cahn-Hilliard equations using the adaptive physics informed neural network, *Commun. Comput. Phys.*, 29 (2021), 930–954.
- [38] H. Xie, C. L. Zhai, X. Xu, et al., A monotone finite volume scheme with fixed stencils for 3D heat conduction equation, *Commun. Comput. Phys.*, 26 (2019), 1118–1142.
- [39] H. Xie, X. Xu, C. L. Zhai, et al., A positivity-preserving finite volume scheme with least square interpolation for 3D anisotropic diffusion equation, *J. Sci. Comput.*, 89(3),(2021), 53.
- [40] F. Xiong, H. Yong, H. Chen, et al., Biot’s equations-based reservoir parameter inversion using deep nerual networks, *J. Geophys. Eng.*, 18 (2021), 862–874.

- [41] H. Yong, P. Song, C. L. Zhai, et al., Numerical simulation of 2-D radiation-drive ignition implosion process, *Commun. Theor. Phys.*, 59 (2013), 737–744.
- [42] G. Yuan, Z. Sheng, Monotone finite volume schemes for diffusion equations on polygonal meshes, *J. Comput. Phys.*, 227 (2008), 6288–6312.
- [43] F. Zhao, X. Lai, G. Yuan, Z. Sheng, A new interpolation for auxiliary unknowns of the monotone finite volume scheme for 3D diffusion equations, *Commun. Comput. Phys.*, 27 (2020), 1201–1233.